Engineering Structures 287 (2023) 116120

Contents lists available at ScienceDirect

Engineering Structures

journal homepage: www.elsevier.com/locate/engstruct

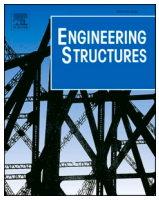

Innovative shear connectors for composite cold-formed steel-timber structures: An experimental investigation

Nathan Vella [a,*], Pinelopi Kyvelou [a], Spiridione Buhagiar [b], Leroy Gardner [a]

[a] Department of Civil and Environmental Engineering, Imperial College London, SW7 2AZ, United Kingdom
[b] Department of Civil and Structural Engineering, University of Malta, MSD 2080, Malta

ARTICLE INFO

Keywords:
Analytical model
Cold-formed steel
Embedment testing
Innovative shear connectors
Load-slip relationship
Push-out testing
Timber particle board

ABSTRACT

An experimental investigation into the behaviour of bespoke shear connectors designed to generate composite action in cold-formed steel-timber structures is presented. The response of the shear connectors was assessed through a comprehensive set of push-out tests, where the cold-formed steel thickness and the connector type and material were varied. Previous studies have shown that while the use of ordinary self-drilling screws as shear connectors enables the development of some composite action, their performance was inhibited by timber embedment. Hence, the main feature of the innovative shear connectors was the introduction of a fitting around the screw to mobilise higher timber embedment forces. The best performing shear connectors achieved about double the shear resistance, four times the initial slip modulus k_s and seven times the mid-range slip modulus $k_{s,m}$ of ordinary self-drilling screws. An analytical model presented in previous research was extended to describe the response of the innovative shear connectors developed in this study. The model was validated against the push-out test results, and shown to be able to accurately predict the ultimate load, slip at ultimate load, and the two slip moduli k_s and $k_{s,m}$ of the innovative connectors, with mean model-to-test ratios of 1.01, 1.15, 1.29 and 1.19 respectively.

1. Introduction

Flooring systems composed of cold-formed steel (CFS) beams supporting timber boards are used extensively in building construction, particularly in industrial and commercial applications. This widespread use can be attributed to the high strength-to-weight ratio of the system, the ease and speed of assembly, and the opportunities for dismantling and reuse [1–3]. The reduction in structural floor weight, combined with the associated material savings for the gravity and lateral load supporting systems, and the potential for reuse, make such flooring systems an attractive, sustainable alternative to traditional solutions [4–5].

Until recently, the design of cold-formed steel – timber (CFS-T) flooring systems was based solely on the properties of the supporting beams, while the timber boards, although physically connected to the underlying beams, were only regarded as an additional permanent load. Studies [6–9] have shown that the benefits of connecting the timber boards to the CFS beams can be significant and that the performance of these systems is strongly related to the resistance, slip modulus and spacing of the shear connectors.

Current practice is for the timber boards to be connected to the underlying CFS beams via self-drilling screws, inserted at regular intervals. The advantage of using such screws is mainly the fast installation process, with the screws being drilled from the top side of the floorboard into the steel, eliminating the need for access to the underside, hence ensuring an intrinsically safe working environment. Initial studies on CFS-T flooring systems have therefore focussed on self-drilling screws used as connectors [6–9], examining how the screw spacing influences the structural behaviour of the system.

Given that the shear connection is key to the efficiency of composite systems, an understanding of the complex interactions at the shear interface between the two constituent components is essential. This has been highlighted in previous research [2–4,10–11], where it was shown that while without an effective connection the system components act independently, with an effective shear connection, slip at the interface is restrained and therefore the system components work together in bending. Previous research carried out on timber-to-timber [12–19], timber-to-concrete [20–26] and timber-to-steel [27] shear connections,

* Corresponding author.
E-mail addresses: n.vella16@imperial.ac.uk (N. Vella), pinelopi.kyvelou11@imperial.ac.uk (P. Kyvelou), spiridione.buhagiar@um.edu.mt (S. Buhagiar), leroy.gardner@imperial.ac.uk (L. Gardner).

https://doi.org/10.1016/j.engstruct.2023.116120
Received 22 January 2023; Received in revised form 15 March 2023; Accepted 5 April 2023
Available online 27 April 2023

motivated the authors to investigate the behaviour of screw connections, comparing perpendicularly driven and inclined screws [28–29]. This research revealed that: (i) any increase in slip modulus should be weighed against the level of difficulty in implementing the connection on-site, (ii) the slip modulus of perpendicularly driven connectors is heavily dependent on timber embedment and connector bending and (iii) the axial pull-through component becomes significant when inclined connectors are installed.

The aim of the present study is to exploit the knowledge gained in previous research to develop high performance shear connectors, bespoke to CFS-T flooring systems, which are easy to install. The performance of the connectors is assessed by means of push-out tests. Note that this study focuses on the performance of the connectors and, therefore, the timber (wood-based particle board) is kept consistent throughout the investigation.

2. Development of innovative connectors

A key criterion that drove the design of the bespoke shear connectors developed herein was to achieve ease of installation. Previous research on inclined shear connectors [28] has established that the on-site installation of inclined connectors is burdensome. When working with inclined self-drilling screws in particular, the tip of the screw is prone to break and become lodged at the interface between the two materials once it comes into contact with the steel sheet. This can overcomplicate and delay installation. It was therefore decided that the connectors examined herein would be perpendicular to the shear interface, with the focus shifted towards achieving enhanced timber embedment resistance and improved connector bending performance. The design of the innovative connectors evolved in parallel with the testing programme, particularly during the initial group of tests, which is described in Section 4.2.

2.1. Type 1 connectors

The first proposed connector, shown in Fig. 1, comprises a screw surrounded by a 20 mm diameter plastic, aluminium or steel fitting, installed into holes predrilled in the timber board. The fittings include a bevelled head, to retain the axial pull-through force component which becomes significant at high values of slip, and a central shaft into which a screw, the same as those used in previous research [28], is inserted. The connection at the interface is achieved by driving the 5.5 mm self-drilling screw into the steel sheet as per normal practice. The proposed configuration aimed at enhancing the timber embedment performance by increasing the area directly in contact with the timber material and therefore reducing the embedment stresses. Note that the decision to test both plastic and metal fittings was based on the embedment test results presented in Section 3, which showed that when a steel shank is embedded into a plastic or steel fitting, which in turn bears into timber, the global embedment properties are essentially independent of the fitting material.

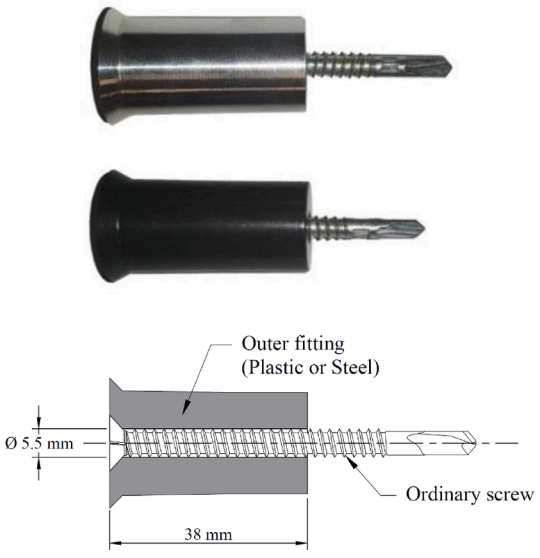

Fig. 1. Type 1 connectors and cross-sectional detail.

2.2. Type 2 connectors

The second type of connector, shown in Fig. 2, consists of a two-part plastic fitting and a 5.5 mm self-drilling screw. The first component of the plastic fitting includes prefabricated slots and is hammered into a predrilled hole in the timber board. The second plastic component is wedged-shaped, and fits around the head of the screw. When the screw is driven into the steel sheet, the wedge-shaped part is forced into the slotted component, further pushing the fitting against the surrounding timber material. The aim of this configuration is to eliminate any gaps between the fitting and the predrilled hole, hence reducing connector rotation.

2.3. Type 3 connectors

The third innovative connector, shown in Fig. 3, includes a fitting similar to that of connector Type 1, but the 5.5 mm screw is replaced by a 5 mm grade 10.9 bolt. The bolt is first inserted into an 8 mm steel shank with a self-locking nut, and then placed into the 20 mm plastic fitting. For this type of connector, 8 mm and 20 mm predrilled holes are required in the steel sheet and timber board respectively. The combined connector is inserted into the predrilled hole in the timber board allowing the steel shank with the self-locking nut to protrude into the 8 mm predrilled hole in the steel sheet. The bolt is then tightened to mobilise the self-locking mechanism. In addition to enhancing the timber embedment force contribution, this configuration aims to transfer the shear and bending stresses onto a larger steel shank (rather than relying on the 5 mm bolt) and to generate a larger sheet bending capacity through the wider grip of the self-locking nut on the steel sheet.

2.4. Type 4 connectors

The fourth innovative connector, shown in Fig. 4, is similar to the third, with the only differences being the type of self-locking mechanism and the transformation of the two-part (steel shank + plastic fitting) component into a single aluminium fitting. As for connector Type 3, predrilling is required in both the timber board and the steel sheet. In this case, upon tightening the bolt, the bevelled circular nut wedges itself into the segmented part of the aluminium fitting, forcing the four segments to open outwards and tighten against the steel sheet. The adoption of a single aluminium fitting in this connector aims to eliminate the tolerance gaps that occur in the multiple component configuration of the third type of connector, though without the beneficial effect of the wider contact with the steel sheet.

2.5. Type 5 connectors

The fifth type of connector, shown in Fig. 5, is similar to the third, but the self-locking nut is replaced by a thick steel washer which is held in place by a standard nut. Predrilling is required, both in the timber board and in the steel sheet. The steel shank still protrudes beyond the lower timber surface and into the steel sheet so that the shear at the interface is transferred directly into the shank, rather than the 5 mm bolt. Note that this configuration was examined in order to determine the maximum stiffness that the shear connection can attain. Adopting a thick washer means that any premature failure due to bending of the steel sheet or bearing of the self-locking nut into the steel sheet is eliminated.

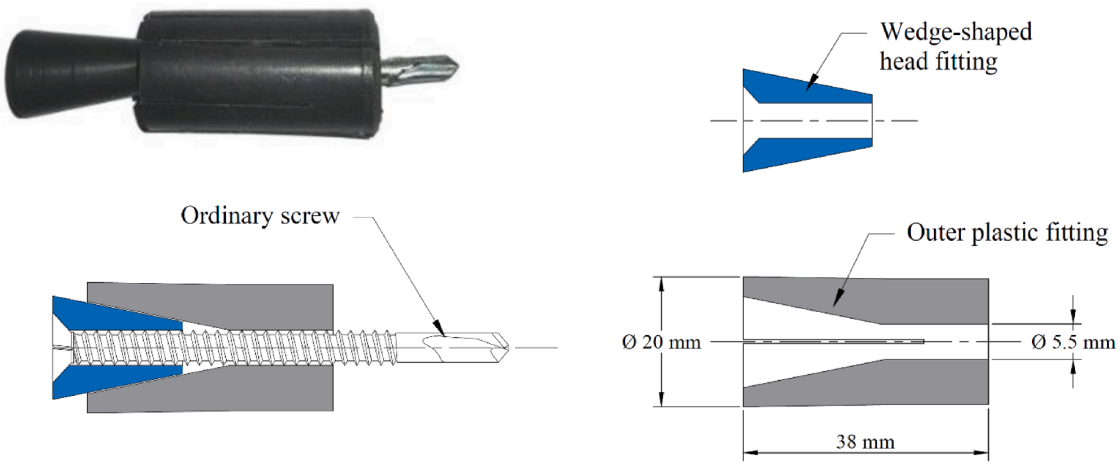

Fig. 2. Type 2 connector including cross-sectional component details and assembly detail.

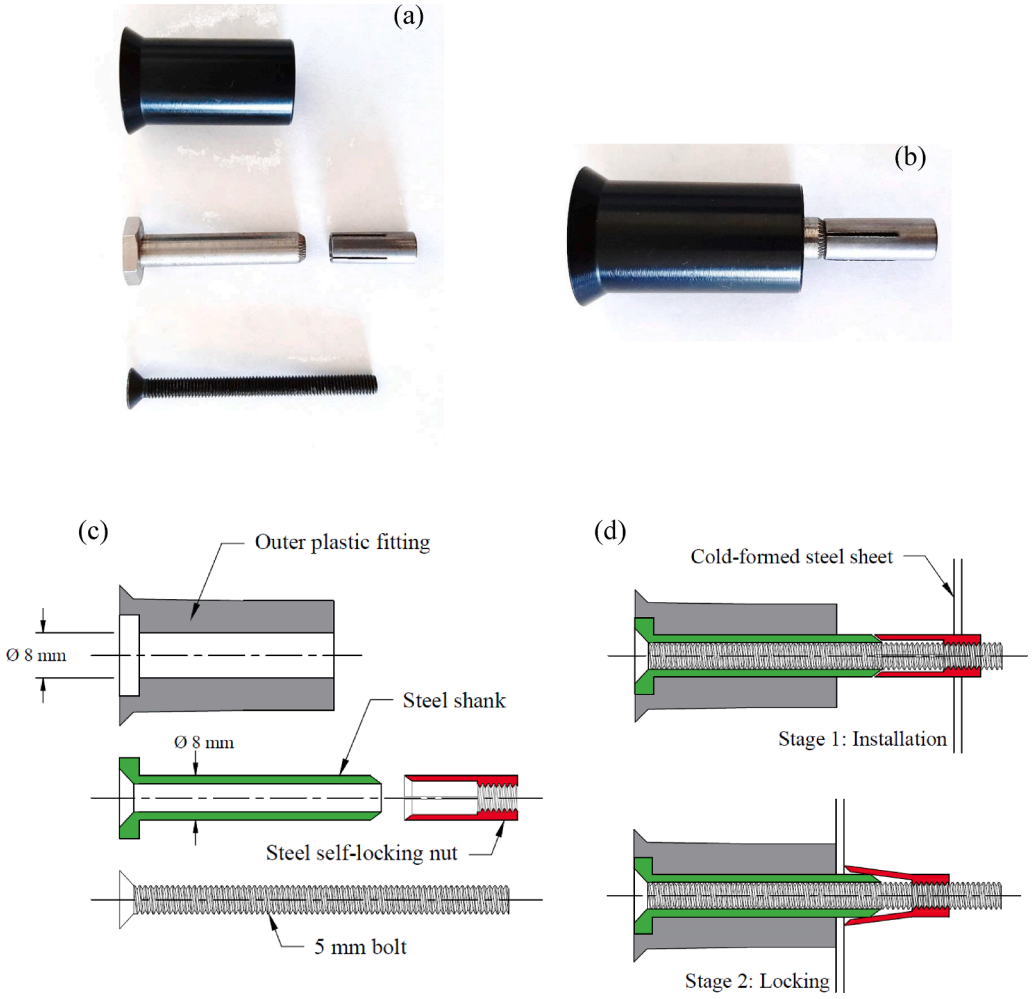

Fig. 3. Type 3 connector (a) Dismantled, (b) Assembled, (c) Cross-sectional details, (d) Assembly detail.

2.6. Type 6 connectors

The sixth connector includes a further modification to the flange of the CFS section in an attempt to limit the connector rotation at the interface. This configuration, shown in Fig. 6 (a), consists of an 8 mm steel shank placed into a 20 mm steel fitting, which is hammered into a predrilled hole in the timber board. The flange of the CFS section is modified with the addition of a second steel plate and a timber infilling block, as shown in Fig. 6 (b). An 8 mm predrilled hole, through all the components of the modified flange, is required for this connector type. The steel shank protrudes into the modified flange section, while a 5 mm bolt clamps and secures the two main components together.

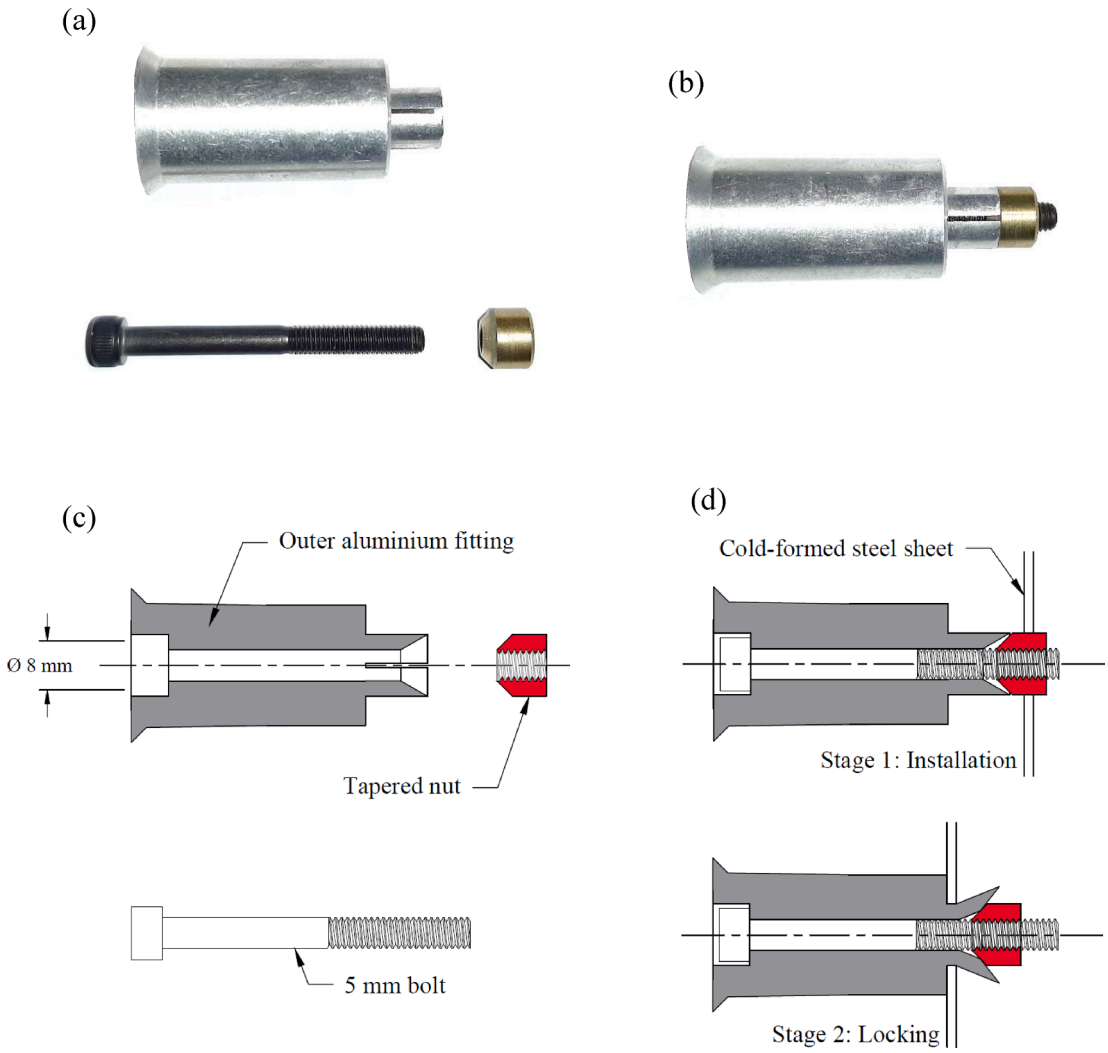

Fig. 4. Type 4 connector: (a) Dismantled, (b) Assembled, (c) Cross-sectional details, (d) Assembly detail.

Fig. 5. Type 5 connector.

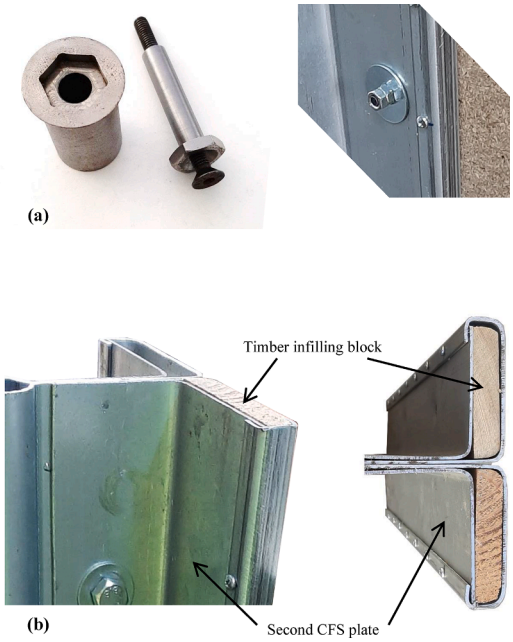

Fig. 6. (a) Type 6 connector, (b) CFS section modification.

3. Embedment tests

Previous research by the authors [28] investigated various interactions between the three components of steel-timber connections, namely, the timber board, the steel section and the connectors. In the present study, it is expected that the embedment stresses exerted on the timber material will be reduced by adopting fittings of larger diameter than the traditionally employed screws, as described in Section 2. According to EN 1995–1-1 [30], the embedment strength f_h of bolted panel-to-timber connections is dependent on the fitting diameter d, with f_h being proportional to $d^{-0.6}$. The accuracy of this equation is confirmed

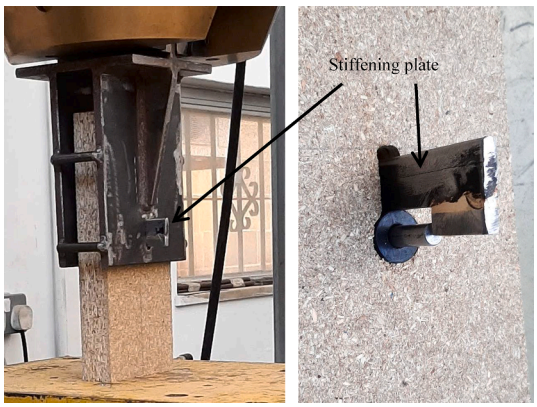

Fig. 7. Embedment test setup.

herein through new embedment tests.

The setup of the embedment tests presented in this study is similar to that described in [28], including a stiffening plate - see Fig. 7 - to minimise connector bending, hence resulting in uniform embedment throughout the timber thickness. Tests were carried out according to EN 383:2007 [31], using a 250 kN Instron 8802 testing machine. Two sets of tests were carried out: in the first set, a plastic fitting with an internal steel shank was employed, while in the second set of tests, the plastic fitting was replaced with a steel fitting. The labelling system of the embedment tests starts with the letters 'EMB', followed by the letters 'P' or 'S' for the plastic or steel fittings respectively and, finally, by the test number.

The average stress-embedment curves for the two sets of tests (i.e. EMB-P_{AV} and EMB-S_{AV}) are presented in Fig. 8, where the stress is defined as the applied load divided by the contact area, namely, the timber thickness t multiplied by the fitting diameter d. The embedment strength f_h and the elastic foundation modulus K_e were determined in line with EN 383:2007 [31] and their values, as obtained from the tests, are presented in Table 1.

Table 1
Particle board embedment test results including average embedment strength and foundation modulus for plastic and steel fittings.

Specimen	f_h (MPa)	K_e (N/mm^3)
EMB - P1	22.4	17.5
EMB - P2	22.8	18.8
EMB - P3	22.7	17.0
EMB - P4	22.0	16.6
EMB - P_{AV}	22.5	17.5
EMB - S1	21.2	30.3
EMB – S2	23.6	28.3
EMB – S3	22.9	21.4
EMB – S4	24.4	26.9
EMB - S_{AV}	23.0	26.7

It is evident from Fig. 8 that the replacement of the plastic fittings with steel fittings had no effect on the embedment strength. Note that the elastic foundation modulus K_e reported in Table 1, has been determined for embedment values lower than 0.5 mm. Thus, although the difference between the K_e values of the two different fittings is significant, its effect on the load–displacement response of the actual connection, where embedments of far beyond 0.5 mm are expected, is small. The curves from the two sets of tests (plastic and steel fittings) are very similar, having an initial linear region followed by a reduction in foundation stiffness at a stress of around 21 MPa. With reference to Table 1, it can be seen that the increase in diameter, from 5.5 mm screws to 20 mm fittings (corresponding to the outer diameter of all innovative connectors studied herein), did result in a reduction in embedment strength, from 42.1 MPa as determined from the screw embedment tests presented in [28] to 22.5 MPa for the plastic fittings and 23.0 MPa for the steel fittings examined herein. This reduction in embedment

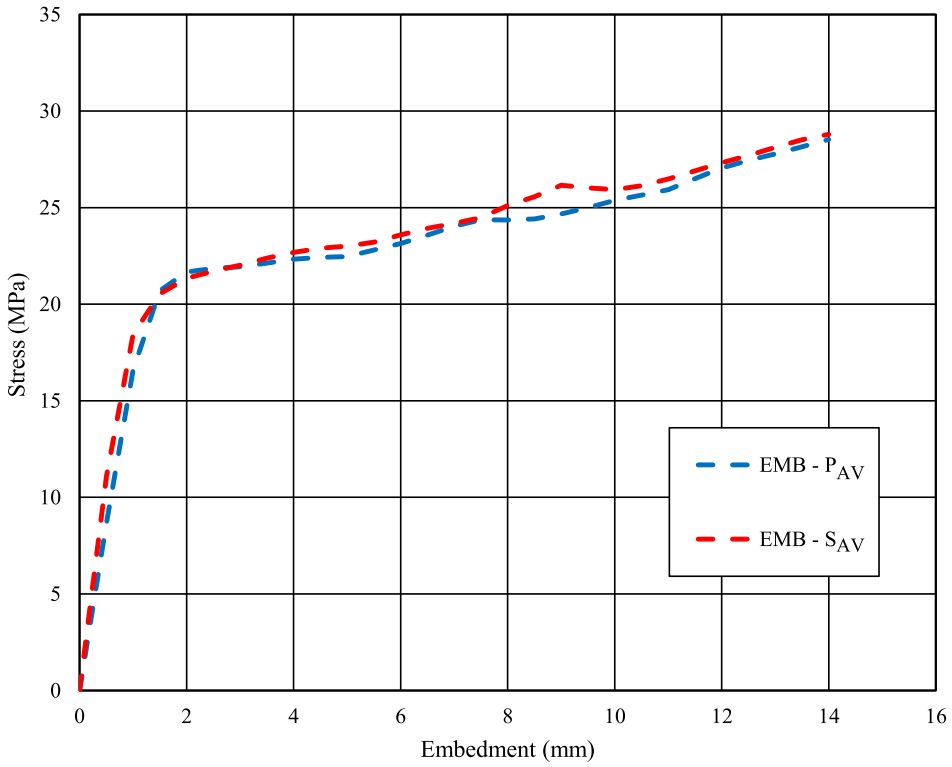

Fig. 8. Average stress-embedment curves for plastic and steel fittings.

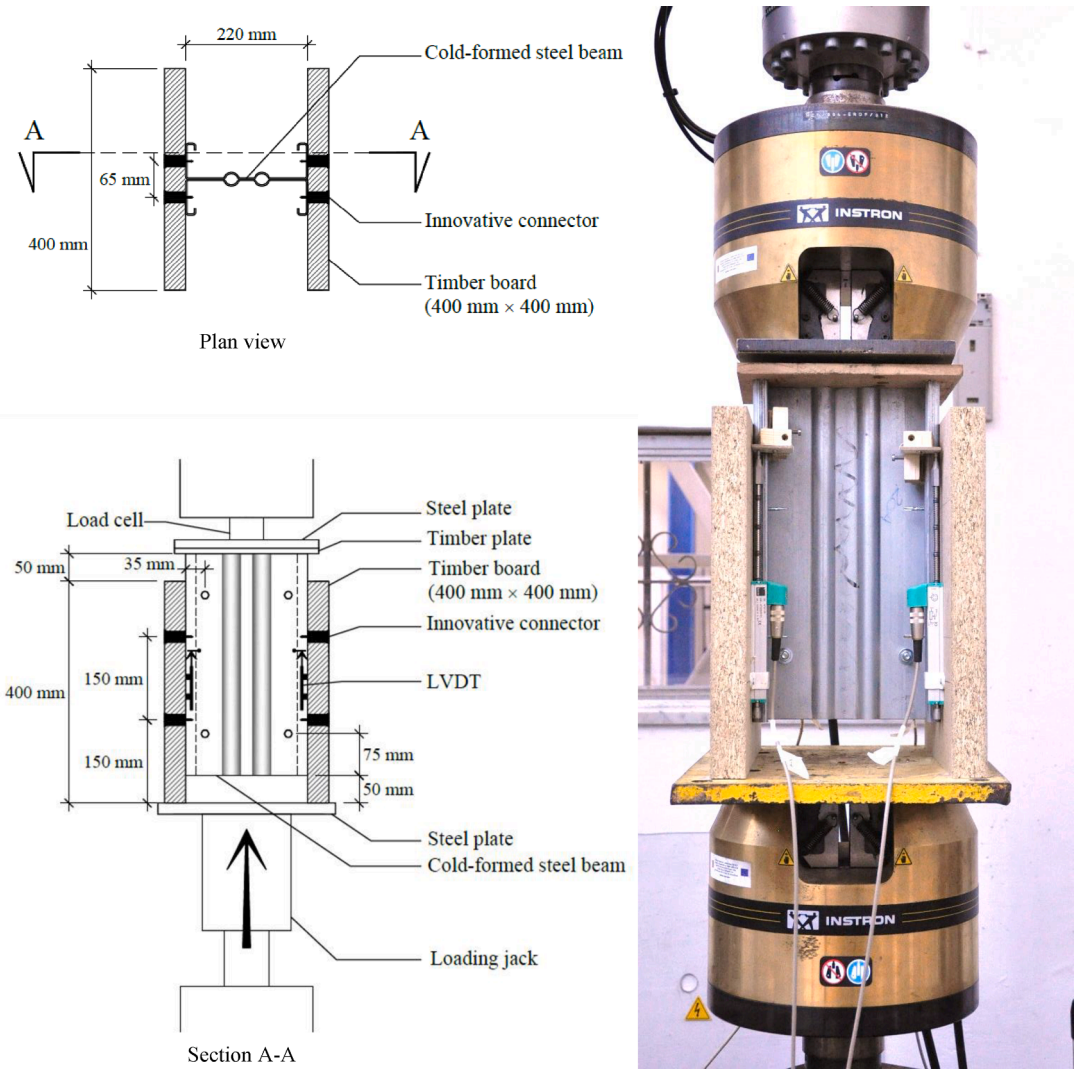

Fig. 9. Push-out test setup.

strength is proportional to around $d^{-0.5}$, which is in close agreement with the $d^{-0.6}$ reduction given in EN 1995–1-1 [30].

4. Push-out tests

The response of the proposed innovative connectors was assessed through a series of push-out tests described in this section. The tests that were carried out as part of this study are divided into two groups: (i) Group 1 tests - an initial set of tests exploring the behaviour of various types of innovative connectors; (ii) Group 2 tests - a comprehensive set of tests carried out on specimens with different fitting materials, steel thicknesses and connector types.

4.1. Test setup and procedure

The specimens consisted of two 400 mm long and 220 mm deep cold-formed, swage beam sections [32] bolted together through the web to form a symmetric I-section. Two CFS thicknesses (i.e. 1.5 mm and 2.0 mm) were investigated in the first group of tests, while thicknesses of 1.5 mm and 2.4 mm were adopted for the second group of push-out tests. Two 400 mm × 400 mm × 38 mm pieces of particle board, taken from the same batch as that described and tested in [28], were then connected to the flanges of the bolted I-section, using four connectors per board. This symmetric setup has been successfully adopted in previous research [28] to ensure concentric loading. The installation of the innovative connectors required pre-drilling into the timber boards. Holes of 20 mm diameter were predrilled using a spade drill bit and then the fittings were hammered into the holes. For the Type 3 to 6 connectors (see Section 2), predrilling in the CFS sheet was also required and, for these four types of fittings, the connectors were tightened with a torque wrench ensuring a uniform torque of 9 Nm per connector.

The ends of the timber boards and the CFS I-section were offset by 50 mm to allow for slippage during the push-out tests, resulting in an initial total specimen height of 450 mm, as shown in Fig. 9. The specimens were tested in a 250 kN Instron 8802 testing machine according to EN 26891 [33], following the loading procedure shown in Fig. 10. The testing was load-controlled up to 70% of the estimated ultimate load and then shifted to displacement-control at a rate of 0.04 mm/s until failure.

The bottom part of the specimens consisted of two 400 mm × 38 mm timber surfaces, which rested directly onto the steel plates of the testing machine. At the top end, a timber spreader plate was placed between the CFS I-section and the testing machine. This meant that the displacement readings could not be extracted directly from the testing machine since the loading jack displacement reading included not only the relative slip between the CFS section and the timber board but also bearing of the CFS I-section into the timber spreader plate. Four linear variable displacement transducers (LVDT) were connected to the timber boards, parallel to, and 15 mm away from, each flange of the CFS I-section. The

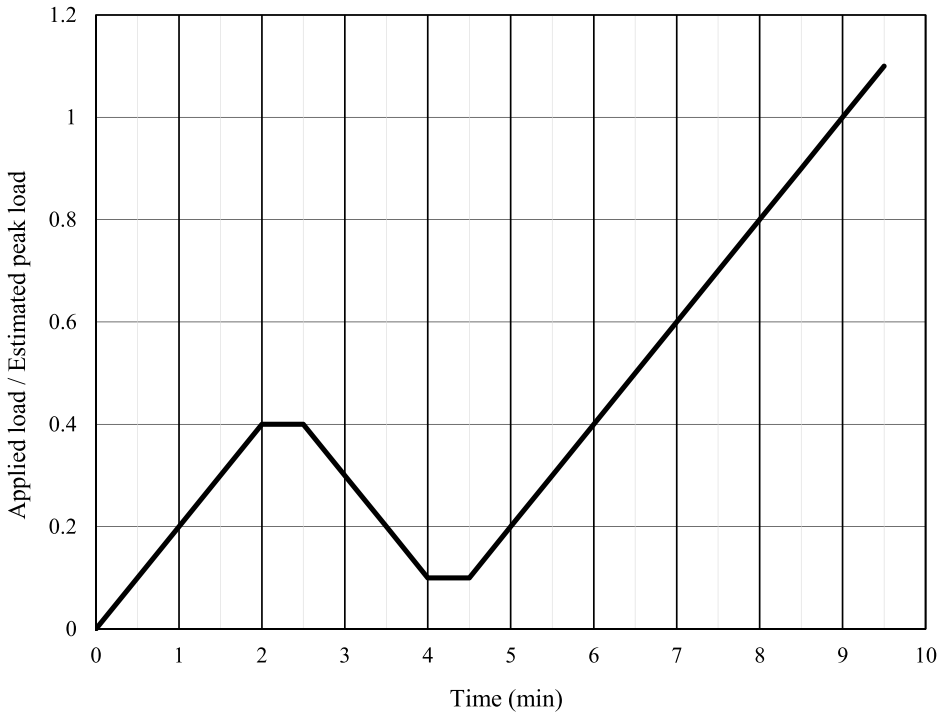

Fig. 10. Push-out test loading procedure - EN 26891 [33].

Table 2
Summary of push-out tests.

Test No.	Specimen designation	Fitting material	Connector type	Connector	Steel sheet thickness (mm)	Test repetitions
01	1-P20-P1	Plastic	Type 1	Screw	2	1
02	1-P20-P2	Plastic	Type 2	Screw	2	1
03	1-P20-A1	Aluminium	Type 1	Screw	2	1
04	1-P20-A4	Aluminium	Type 4	Bolt	2	1
05	1-P15-P3	Plastic	Type 3	Bolt	1.5	1
06	1-P15-P5	Plastic	Type 5	Bolt	1.5	1
07	1-P15-S5	Steel	Type 5	Bolt	1.5	1
08	1-P15-S6	Steel	Type 6	Bolt	1.5	1
09	2-P15-P1	Plastic	Type 1	Screw	1.5	2
10	2-P24-P1	Plastic	Type 1	Screw	2.4	2
11	2-P15-P3	Plastic	Type 3	Bolt	1.5	2
12	2-P24-P3	Plastic	Type 3	Bolt	2.4	2
13	2-P15-P5	Plastic	Type 5	Bolt	1.5	2
14	2-P24-P5	Plastic	Type 5	Bolt	2.4	2
15	2-P15-S1	Steel	Type 1	Screw	1.5	2
16	2-P24-S1	Steel	Type 1	Screw	2.4	2
17	2-P15-A4	Aluminium	Type 4	Bolt	1.5	2
18	2-P24-A4	Aluminium	Type 4	Bolt	2.4	2
19	2-P15-S5	Steel	Type 5	Bolt	1.5	2
20	2-P24-S5	Steel	Type 5	Bolt	2.4	2

tip of each LVDT bore onto a fitting, which was in turn secured onto the CFS flange. This setup ensured that the displacement readings captured the relative slip between the timber boards and the CFS section, while excluding any movement due to bearing occurring at the contact points between the specimen and the testing machine.

The labelling system adopted for the push-out tests starts with the number '1' or '2' to identify whether the specimen belongs to the first or second group of tests. This is followed by the letter 'P' and the number '15', '20' or '24' to indicate whether the push-out test was carried out using 1.5, 2.0 or 2.4 mm thick CFS. Finally, the last part of the label refers to the shear connection employed where the letters 'P', 'S' or 'A' refer to the fitting material (plastic, steel or aluminium respectively), followed by the number corresponding to the connector type as defined in Section 2. A full list of the conducted push-out tests is given in Table 2.

4.2. Group 1 tests

The aim of the Group 1 tests was to develop an understanding of the load-slip behaviour and ease of installation of the different bespoke connectors. The outer shape of all the fittings used in these tests featured a bevelled head and a constant fitting diameter of 20 mm, as shown in Fig. 11 (a), except for the Type 2 connectors, which featured a constant fitting diameter of 20 mm - see Fig. 11 (b). The design of the connectors evolved in parallel with this phase of the testing programme and the obtained results helped to guide the testing schedule for the second group of tests.

The interface shear force ($F_{is,t}$) – slip ($\delta_{is,t}$) curves for the first set of tests are shown in Fig. 12. The maximum load per connector $F_{v,t}$, the slip at the maximum load $\delta_{is,u,t}$, the slip modulus $k_{s,t}$ as defined in EN 26891 [33], the mid-range slip modulus $k_{s,m,t}$ and the failure mode for all Group

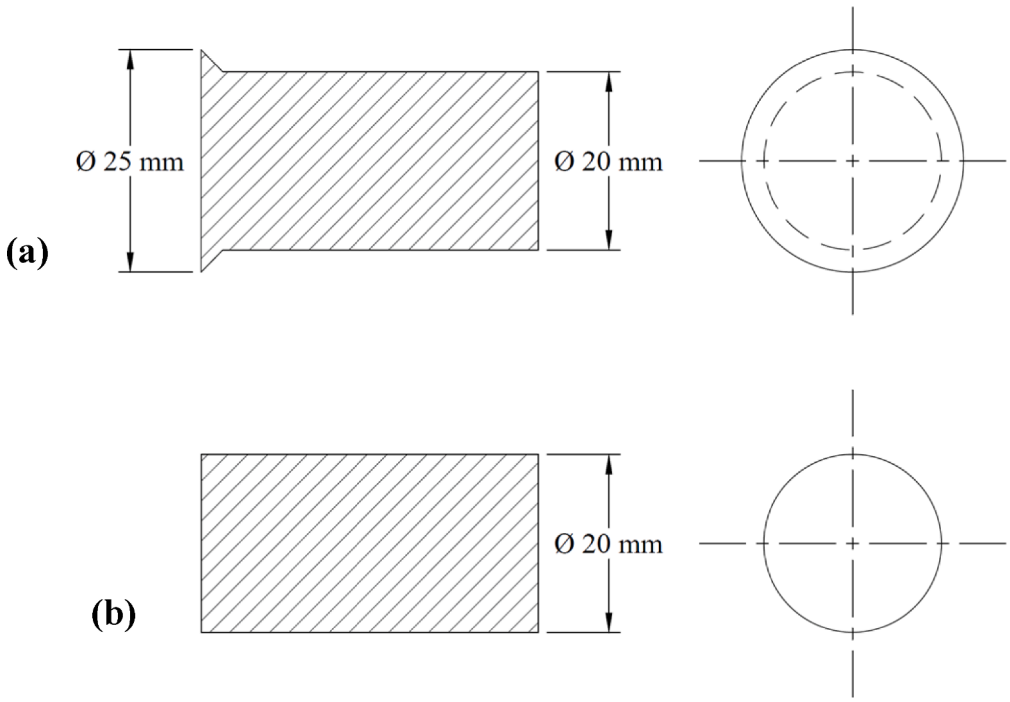

Fig. 11. Outer fitting dimensions for (a) Types 1, 3–6 connectors and (b) Type 2 connector.

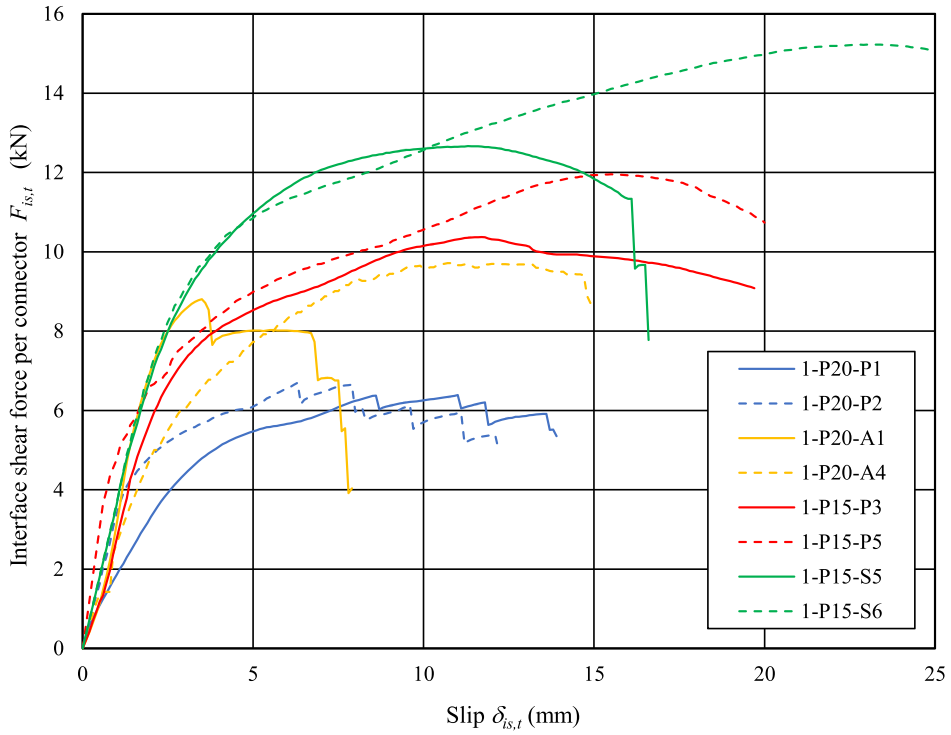

Fig. 12. Force-slip curves for Group 1 push-out tests (Tests 01–08).

1 tests are presented in Table 3. The slip moduli $k_{s,t}$ were determined using the force and slip values extracted at 10% and 40% of the estimated maximum load, while the mid-range slip modulus $k_{s,m,t}$ was evaluated using the values at 40% and 70% of the estimated maximum load. Adopting a single value for the estimated maximum load throughout a set of tests ensures that the slip moduli are evaluated at the same load levels, hence enabling a fair comparison between the results. For this set of tests, the estimated ultimate load was taken as 8.5 kN.

It can be seen from Table 3 that both the ultimate load and stiffness increased when the plastic fitting was replaced by an aluminium fitting. It is also evident that the introduction of the self-locking device led to higher loads and, in the case of plastic fittings, also resulted in a higher 40–70% slip modulus. The specimens that featured a thick washer to locally stiffen the cold-formed steel section reached the highest ultimate

Table 3
Group 1 - Push-out test results.

Specimen designation	$F_{v,t}$ (kN)	$\delta_{is,u,t}$ (mm)	$k_{s,t}$ (N/mm)	$k_{s,m,t}$ (N/mm)	Failure mode
1-P20-P1	6.70	6.3	3473	778	1, 2
1-P20-P2	6.39	11.0	1551	498	6
1-P20-A1	8.81	3.5	3938	4457	1
1-P20-A4	9.73	10.9	2500	1704	4, 5
1-P15-P3	10.37	11.7	3189	2778	4, 7
1-P15-P5	11.96	15.5	6121	2266	3, 1
1-P15-S5	12.67	11.3	3603	3453	1, 4
1-P15-S6	15.23	23.1	3656	3649	4, 3

Failure mode key: 1 = Screw / bolt failure; 2 = Fitting failure; 3 = Pull-through failure; 4 = Fitting rotation; 5 = Failure of locking device; 6 = Screw bearing into fitting; 7 = Locking device bearing into steel sheet.

Fig. 13. Failure of specimen 1-P20-P2 – screw bearing into the preformed slots.

Fig. 14. Failure of specimen 1-P15-P3 – locking nut bearing into the steel sheet.

loads and slip moduli.

Overall, the best performing connection was the sixth type (1-P15-S6). However, since its configuration involved doubling the CFS flange and inserting a timber infilling block, its installation was deemed to be unsuitable for practical application. This configuration was therefore omitted from the second group of tests. Furthermore, since the second connector (1-P20-P2) performed poorly due to the screw bearing into the preformed slots in the plastic fitting as shown in Fig. 13, this fitting was also omitted from the second group of tests.

The third type of connector (1-P15-P3) performed relatively well, achieving high ultimate loads and slip moduli. It was observed however, in the first set of tests, that the segments of the self-locking nut did not open sufficiently, thus leading to the nut bearing into the steel sheet as shown in Fig. 14. The connector was therefore modified for the second set of tests by introducing a longer steel shank within the plastic fitting. The longer shank meant that the four segments of the self-locking nut would open into a larger radius and come into contact with the CFS sheet further away from the outer surface of the shank, thus minimising the risk of the segments bearing into the CFS sheet.

Note that for this exploratory group of tests, both the outer diameter of the fittings and the predrilled holes in the timber boards were 20 mm. However, in some instances, the fitting became lodged in the timber before reaching the full installation depth; in these cases, the hole had to be widened slightly. Therefore, for the Group 2 tests, the diameter of the predrilled holes was kept at 20 mm, but the fittings were modified as shown in Fig. 15, with a smaller diameter at the tail end of the fitting to facilitate installation.

4.3. Group 2 tests

4.3.1. Introduction

Following the exploratory Group 1 tests, a comprehensive set of tests with two repeats per specimen was carried out on the connectors that were deemed worthy of further investigation. Based on the observations from the Group 1 tests, the outer shape of the fittings for all Group 2 tests consisted of a bevelled head followed by a cylinder of 20.1 mm diameter towards the head end narrowing down to a 19.5 mm towards the tail end as shown in Fig. 15. This simplified the installation process and ensured a tight fit between the fitting and the timber board at the head end.

The interface shear force ($F_{is,t}$) – slip ($\delta_{is,t}$) curves for all Group 2 test specimens, including two ordinary screw specimens tested in [28], P15B-00W – consisting of ordinary winged screws driven perpendicularly into timber particle board and 1.5 mm CFS, and P24B-45N – consisting of ordinary non-winged screws driven at 45° into timber particle board and 2.4 mm CFS, are shown in Fig. 16. The experimentally determined values for $F_{v,t}$, $\delta_{is,u,t}$, $k_{s,t}$, $k_{s,m,t}$ and the failure modes are presented in Table 4. The slip moduli were evaluated as described in Section 4.2 for an estimated ultimate load of 8.5 kN.

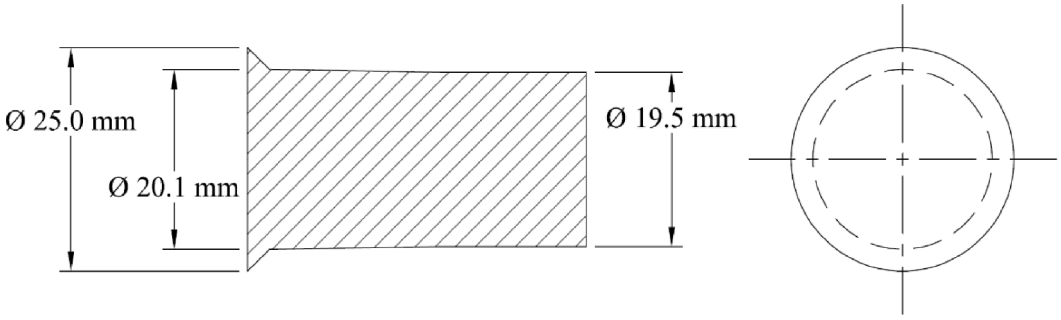

Fig. 15. Modified outer fitting dimensions for Group 2 tests.

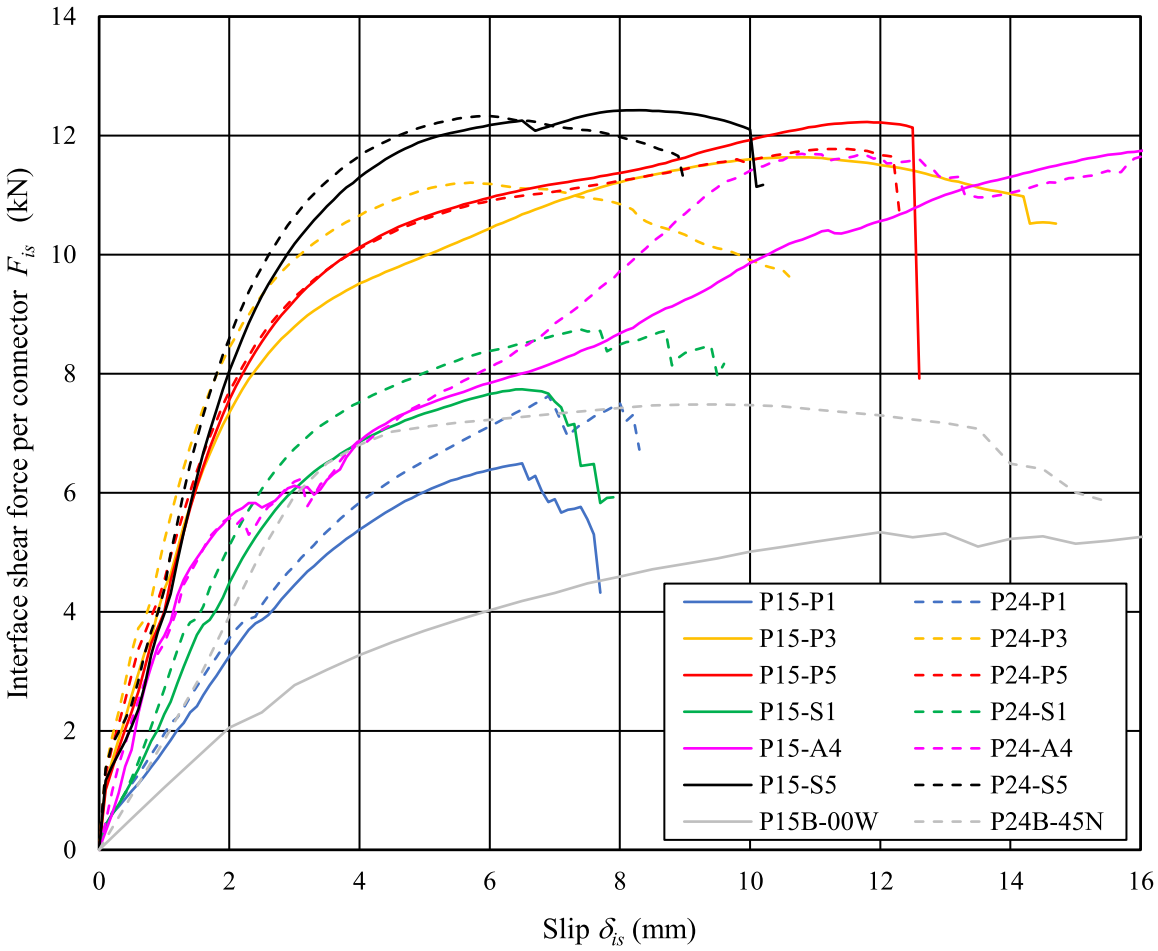

Fig. 16. Force-slip curves for all Group 2 push-out tests (Tests 9–20) including curves for specimens with ordinary screws –P15B-00W and P24B-45N,as presented in [28].

Table 4
Group 2 - Push-out test results.

Specimen designation	$F_{v,t}$ (kN)	$\delta_{is,u,,t}$ (mm)	$k_{s,t}$ (N/mm)	$k_{s,m,t}$ (N/mm)	Failure mode
2-P15-P1	6.49	6.5	1496	914	3, 6
2-P24-P1	7.63	6.9	1632	1143	3, 6
2-P15-P3	11.63	10.5	3681	3481	1, 2
2-P24-P3	11.21	5.7	4907	3878	7, 1
2-P15-P5	12.23	11.8	3510	3787	1/2, 3
2-P24-P5	11.77	11.5	4206	3320	1/2, 3
2-P15-S1	7.74	6.5	2346	1739	1, 4
2-P24-S1	8.74	7.4	2876	2107	1, 4
2-P15-A4	11.80	16.9	4110	1341	1, 7
2-P24-A4	11.78	17.4	3117	1395	1, 7
2-P15-S5	12.43	8.3	3016	4192	1, 3
2-P24-S5	12.33	5.9	3215	4527	1, 3

Failure mode key: 1 = Fitting rotation; 2 = Pull-through failure; 3 = Screw / bolt bending failure; 4 = Screw / bolt shear failure; 5 = Thread failure; 6 = Fitting failure; 7 = Failure of locking device.

4.3.2. Results and observations

With reference to Fig. 16 and Table 4, it is evident that the specimens employing the Type 1 connectors exhibited the poorest performance both in terms of ultimate load and stiffness, and failed in the screws. For the plastic fittings, namely 2-P15-P1 and 2-P24-P1, failure by splitting close to the interface was observed, as shown in Fig. 17, allowing the screw to bend within the length of the fitting. This observation also explains why the specimens with the Type 1 connectors with plastic fittings reached lower ultimate loads and slip moduli than their steel counterparts. It should be also mentioned that for the specimens with the Type 1 connectors, increasing the CFS thickness resulted in an increase in both the strength and stiffness of the connection.

The specimens with self-locking connectors, namely Types 3 and 4, performed generally well. Tests involving the Type 3 connectors, which included a plastic outer fitting, reached ultimate loads comparable to those achieved by the specimens with the Type 5 connectors and plastic fittings, while reaching even higher slip moduli. Failure in this case depended on the thickness of the CFS sheet. For the 1.5 mm thick CFS specimens, the fitting rotated and pulled through the timber board, as shown in Fig. 18, while for the 2.4 mm thick CFS specimens, failure was initiated by bending of the four segments of the locking nut, as shown in Fig. 19.

The specimens with the second type of self-locking connector, Type 4, achieved initial slip moduli comparable to those with the Type 3 connectors, but it is evident from both Fig. 16 and Table 4, that the specimens experienced a sudden reduction in stiffness at a load of around 5.5 kN. A review of close-up video recordings of the tests revealed that this sudden reduction in stiffness was caused by the failure of the four segments that locked the connector against the CFS section; this was followed by the bevelled circular nut pulling into the CFS sheet, as shown in Fig. 20. Increasing the CFS thickness had no effect on the performance of this type of connector. Although the specimens with these connectors reached high ultimate loads, the sudden reduction in stiffness is undesirable for practical applications.

The specimens with the Type 5 connectors reached the highest ultimate loads, while their slip moduli were among the highest achieved,

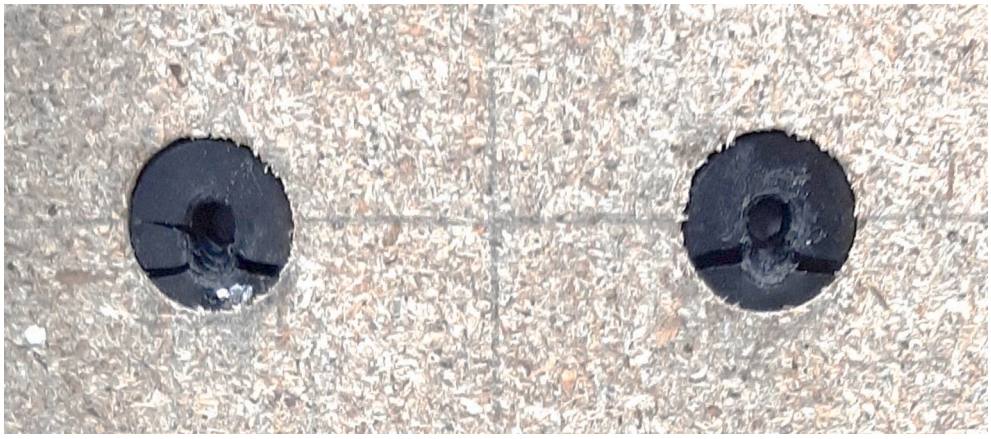

Fig. 17. Failure of specimens 2-P15-P1 and 2-P24-P1 showing the split fittings.

Fig. 18. Rotation and pull-through failure of specimen 2-P15-P3.

only being surpassed by the specimens with the Type 3 connectors. Again, the CFS thickness had no significant effect on the performance of the connectors. The Type 5 connectors require access to the underside of the CFS beams for their installation, which is undesirable for practical applications.

Table 5 shows a comparison between the Group 2 test results and the results obtained from push-out tests on specimens with ordinary screws driven perpendicular to the shear interface, presented in [28]. It is evident from this comparison that, although the Type 1 connectors gave

Fig. 20. Failure of the Type 4 connector - failure of the four locking segments followed by the bevelled nut pulling into the CFS sheet.

Table 5
Comparison of Group 2 push-out test results with ordinary screw specimen results – P15B-00W and P24B-00W, as presented in [28].

Specimen designation	$F_{v,t}$ (kN)	$F_{v,t}/F_{v,t\text{-}ref}$	$k_{s,t}$ (N/mm)	$k_{s,t}/k_{s,t\text{-}ref}$	$k_{s,m,t}$ (N/mm)	$k_{s,m,t}/k_{s,m,t\text{-}ref}$
P15B-00W [11]	5.57		984		502	
2-P15-P1	6.49	1.17	1496	1.52	914	1.82
2-P15-P3	11.63	2.09	3681	3.74	3481	6.93
2-P15-P5	12.23	2.20	3510	3.57	3787	7.54
2-P15-S1	7.74	1.39	2346	2.38	1739	3.46
2-P15-A4	11.80	2.12	4110	4.18	1341	2.67
2-P15-S5	12.43	2.23	3016	3.07	4192	8.35
P24B-00W [11]	7.05		1236		621	
2-P24-P1	7.63	1.08	1632	1.32	1143	1.84
2-P24-P3	11.21	1.59	4907	3.97	3878	6.24
2-P24-P5	11.77	1.67	4206	3.40	3320	5.35
2-P24-S1	8.74	1.24	2876	2.33	2107	3.39
2-P24-A4	11.78	1.67	3117	2.52	1395	2.25
2-P24-S5	12.33	1.75	3215	2.60	4527	7.29

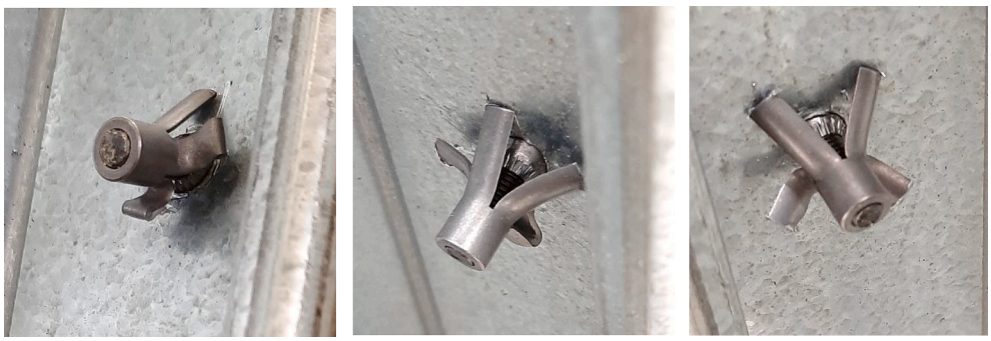

Fig. 19. Failure of specimen 2-P24-P3 showing bending of the four segments of the locking nut.

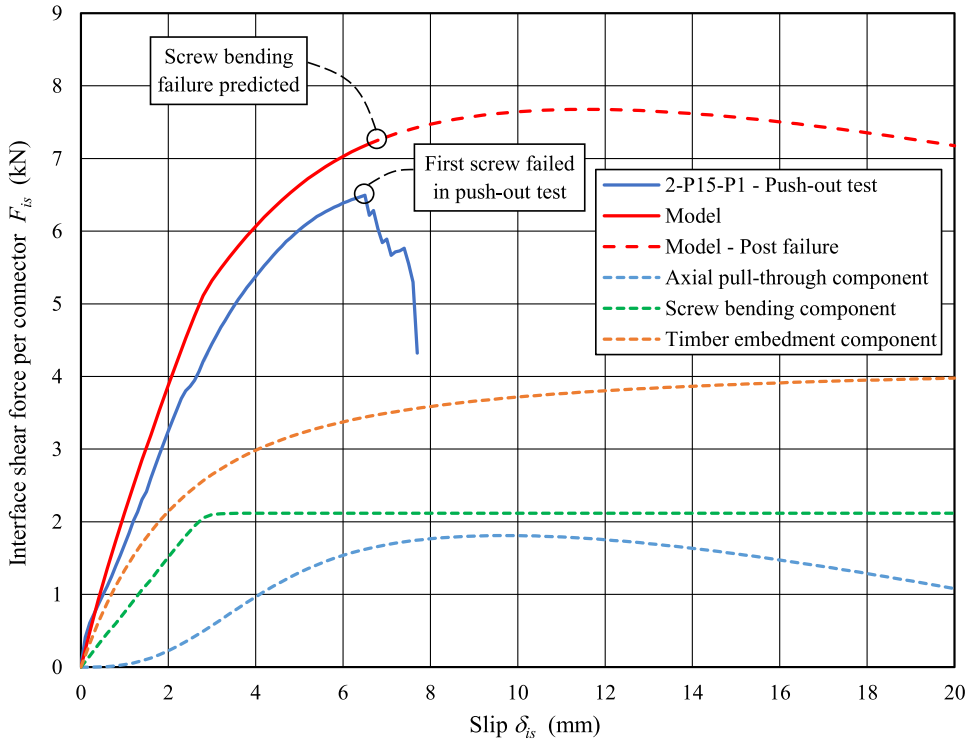

Fig. 21. Analytical prediction of the force-slip curve for specimen 2-P15-P1.

the lowest improvements over the reference ordinary screws, these still reached ultimate load increases of up to 17% and 39% for the plastic and steel fittings respectively, while the slip moduli $k_{s,t}$ and $k_{s,m,t}$ increased by up to around 50% and 80% respectively for the plastic fittings and 140% and 250% respectively for the steel fittings. Such improvements are significant, especially when considering the relative ease with which these types of connectors were installed. Note that the achieved strength and stiffness improvements were generally greater for the specimens comprising the thinner steel sections (i.e. 1.5 mm).

Overall, the best performing connector was Type 3, due to both its easy assembly on site and improved performance. This connector is relatively easy to install, requiring no access to the underside of the CFS section thanks to the self-locking nut. Specimens with this type of connector achieved improvements in ultimate load of up to around 110% and increases in slip moduli $k_{s,t}$ and $k_{s,m,t}$ of up to around 300% and 600% respectively.

5. Analytical modelling

An analytical model describing the load (F_{is})-slip (δ_{is}) response of cold-formed steel-to-timber screw connections was established in [29]. The model involved the determination of three force components: (i) timber embedment F_{emb}, (ii) screw bending F_{bm} and (iii) axial pull-through F_{pt}.

Separate force-slip relationships are first defined for each individual force component, accounting for timber damage, partially driven screws and the initial screw inclination from the normal to the shear plane. The slip values are then varied incrementally in each individual relationship to determine the change in force associated with each of the three force components. Slip values for each increment are kept consistent throughout the individual force component calculations, thus the summation of the resulting forces after each increment, as presented in Eq. (1), may be associated with a specific value of slip δ_{is}.

$$F_{is} = F_{emb} + F_{bm} + F_{pt} \quad (1)$$

In this section, the aforementioned model is extended to cater for the bespoke connectors investigated herein, to facilitate their use in CFS-T composite construction. All experimental data used in this section are from the Group 2 tests described in Section 4.3.

5.1. Extension of model for innovative connectors

5.1.1. Extension of the embedment and screw bending components

During the first two tests, 2-P15-P1 and 2-P24-P1, it was observed that the plastic fitting split, allowing the screw to bend within the width of the fitting, as described in Section 4.3.1. The behaviour and failure mode of these two specimens was very similar to those presented in [29], implying that the same model may be used without the need for modification. Fig. 21 shows the load-slip curve generated by the analytical model for 2-P15-P1 in comparison to the curve obtained from the push-out test. The three force components contributing to the predicted analytical curve are also shown in Fig. 21.

For all other specimens, bending of the screw or bolt within the fitting was restrained and could therefore only occur at the interface between the CFS section and the timber board. Any displacements of the connectors within the timber board, resulting in timber embedment, are attributed to rotation of the fittings. Thus, the plastic hinge location defined in the original model [29], which was key to the calculation of the individual force components, is now replaced by the pivoting point of the fitting.

The pivoting point can be determined by defining the stress state that the shearing force at the interface generates on the timber surrounding the fitting. This procedure requires the determination of the 2-dimensional projected shape of the fitting, defining area A, shown by the red dashed lines in Fig. 22. This area is subsequently used to determine the distance between the centroid of the 2-dimensional projection of the fitting and the shear interface y_t, and the two elastic section moduli about the centroidal axis $W_{el,\min}$ and $W_{el,\max}$, taking into account the bevelled head and the stiffer foundation material towards the outer surface of the timber board, as shown in Fig. 22.

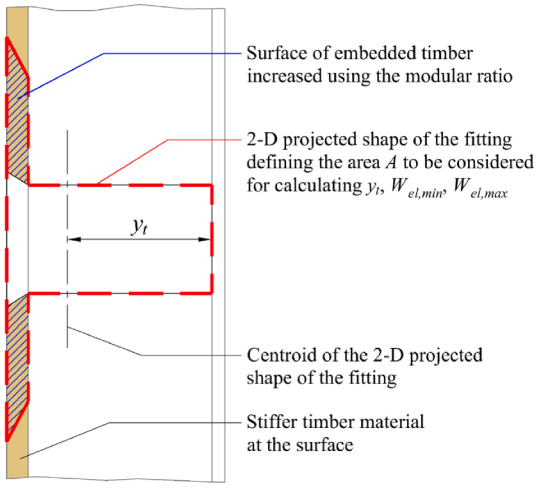

Fig. 22. 2-Dimensional projected surface of the fitting defining the area A (red dashed line) to be considered for calculating y_t, $W_{el,\min}$ and $W_{el,\max}$.

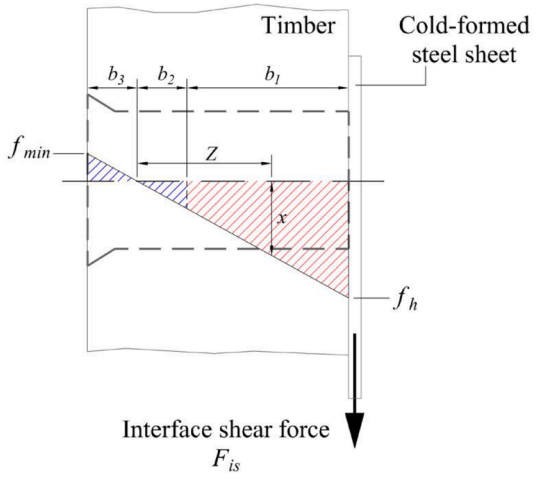

Fig. 23. Embedding stresses generated on the timber surface due to fitting rotation caused by the applied interface shear force.

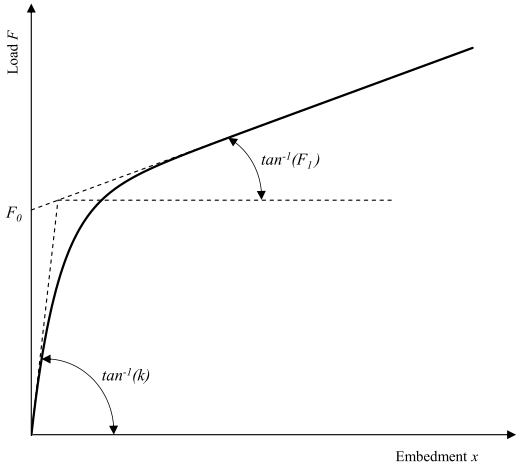

Fig. 24. Nonlinear foundation model proposed by Foschi [36].

The maximum bending capacity of the CFS sheet is then calculated as described in [29] using Eq. (2), as a function of the thickness of the CFS sheet t, its yield strength f_y and the diameter d of the screw or the steel shank passing through and bearing onto the CFS sheet:

$$M_{pl,cfs} = \frac{\alpha d t^2}{4} f_y \tag{2}$$

The equation above includes the parameter α, which considers the extent of the steel sheet being mobilised when subjected to bending and bearing by a dowel, as a factor of the diameter of the dowel (screw or steel shank in this investigation). To determine the appropriate values of the parameter α, reference was made to the expression proposed by Teh and Uz [34] defining the ultimate capacity of a steel sheet, subjected to a bolt induced 'bearing and tiling' failure mode, in terms of the net steel sheet width W_n, the bolt diameter, the thickness of the steel sheet and the ultimate strength of the steel sheet. This expression has been used to determine the steel sheet 'bearing and tilting' capacity for the two steel thicknesses being investigated, with the results substituted in the bearing resistance expression defined in Table 8.2 of EN 1993-1-3 [35] to determine the values of α. The resulting values have been used in this investigation and are equal to 2.7 for the 1.5 mm steel and 3.1 for the 2.4 mm steel.

Having determined the geometric properties of the 2-dimensional projected area of the fitting and the maximum bending capacity of the CFS sheet, the force F required at the interface to generate a stress equal to the timber embedment strength f_h may be determined by rewriting the maximum compressive stress expression of the timber board given by Eq. (3):

$$f_h = \frac{F}{A} + \frac{F y_t}{W_{el,min}} - \frac{M_{pl,cfs}}{W_{el,min}} \tag{3}$$

to give:

$$F = \frac{f_h + \frac{M_{pl,cfs}}{W_{el,min}}}{\frac{1}{A} + \frac{y_t}{W_{el,min}}} \tag{4}$$

Following the determination of F, Eq. (5) can be used to calculate the minimum compressive (or maximum tensile) stress f_{min}.

$$f_{min} = \frac{F}{A} - \frac{F y_t}{W_{el,max}} + \frac{M_{pl,cfs}}{W_{el,max}} \tag{5}$$

The stresses f_h and f_{min} define the stresses at the two surfaces of the timber board, as shown in Fig. 23. Considering, as a simplification, that the base lengths b_3 and b_2 of the two self-equilibrating stress fields shown in Fig. 23 are equal, the force F_{emb} required to embed the fitting into the timber can be found using the nonlinear foundation model proposed by Foschi [36] as defined in Eq. (6):

$$F = (F_0 + F_1 x)\left(1 - e^{(-kx)/F_0}\right) \tag{6}$$

leading to the integral in Eq. (7):

$$F_{emb} = \int_0^{b_1+b_2} \left(F_0 + F_1 \frac{\delta_{is}}{b_1+b_2} Z\right)\left(1 - e^{\left(\frac{-k\delta_{is}Z}{F_0(b_1+b_2)}\right)}\right) dz - \int_0^{b_2} \left(F_0 + F_1 \frac{x_o}{b_2} Z\right)\left(1 - e^{\left(\frac{-kx_oZ}{F_0 b_2}\right)}\right) dz \tag{7}$$

and the solution to the integral given in Eq. (8) [29]:

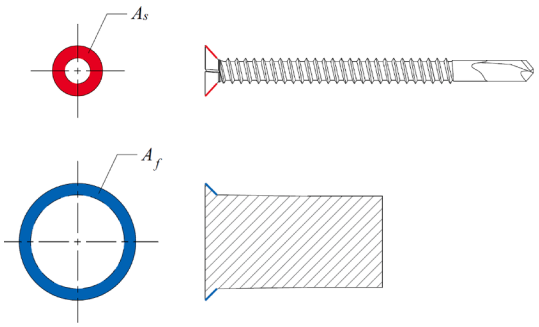

Fig. 25. Definition of head bearing areas.

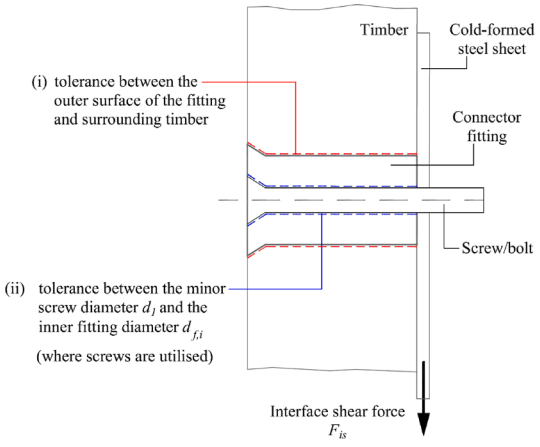

Fig. 26. Tolerances along contact boundaries.

$$F_{emb} = \frac{b_1 + b_2}{2k^2}\left[F_1 k^2 \delta_{is} - \frac{2F_0{}^2\left(e^{\left(\frac{k\delta_{is}}{F_0}\right)} - 1\right)(k + F_1)}{\delta_{is} e^{\left(\frac{k\delta_{is}}{F_0}\right)}} + 2kF_0\left(k + \frac{F_1}{e^{\left(\frac{k\delta_{is}}{F_0}\right)}}\right)\right]$$
$$-\frac{b_2}{2k^2}\left[F_1 k^2 x_0 - \frac{2F_0{}^2\left(e^{\left(\frac{kx_0}{F_0}\right)} - 1\right)(k + F_1)}{x_0 e^{\left(\frac{kx_0}{F_0}\right)}} + 2kF_0\left(k + \frac{F_1}{e^{\left(\frac{kx_0}{F_0}\right)}}\right)\right] \quad (8)$$

As shown in Fig. 23, the distance b_1 is the effective embedment length in the timber and the variable Z is measured from the pivoting point of the fitting. F_0, F_1 and k are parameters of the nonlinear foundation model proposed by Foschi [36] as illustrated in Fig. 24, representing the y-intercept, the slope of the asymptote and the initial stiffness per unit length of the dowel respectively, while x is the displacement or embedment into the timber.

Given that the types of connectors described above restrain bending of the screw or bolt within the fitting, the only bending force component is that generated on the CFS sheet at the interface when the fitting starts rotating. This, however, is already taken into account when determining the stresses at the extreme timber fibres in Eqs. (3) to (5) and therefore no additional force components due to bending need to be considered.

5.1.2. *Extension of the axial pull-through component*

The axial pull-through component in [29] was defined using the three-parameter function proposed by Foschi [36], as presented in Eq. (6). Pull-through tests presented in [28] showed that the load–displacement relationship is characterised by an initial ramping-up region followed by a plateau, implying that the stress is independent of displacement beyond the ramping-up region. As described in Section 4.1, all bolted specimens were secured by a torque of 9 Nm per bolt applied using a torque wrench, preloading the bolt beyond the initial linear region of the pull-through load–displacement relationship. Therefore, for the examined connectors, the pull-through relationship may be reduced to a constant force, equal to the value of the force on the aforementioned plateau.

The adopted plateau force value was determined based on the screw

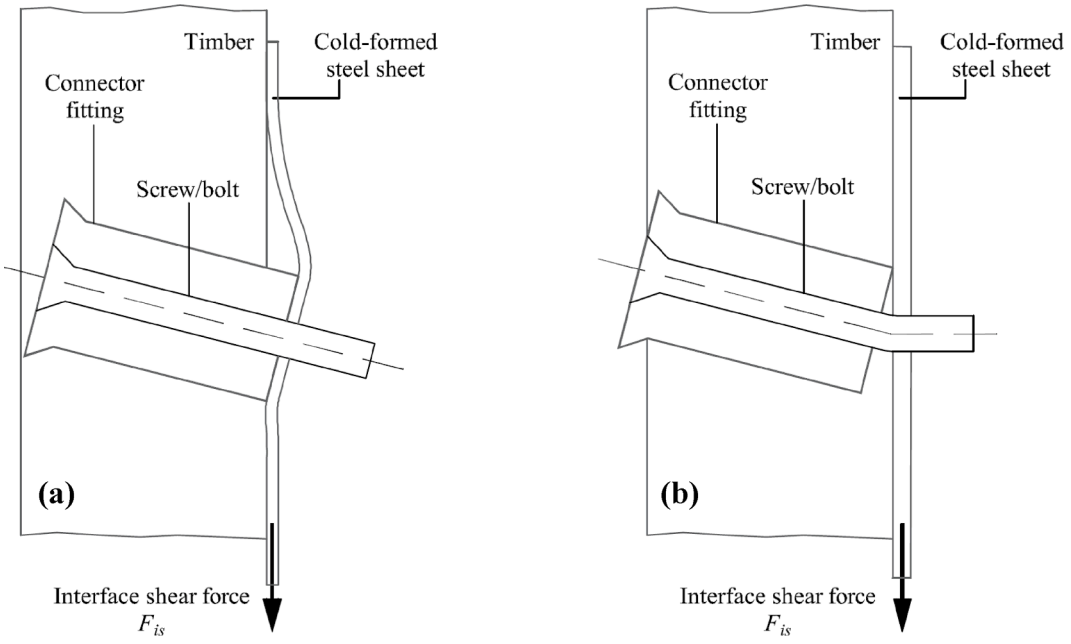

Fig. 27. (a) Rotation of the fitting due to CFS sheet bending, (b) Rotation of the fitting due to screw/bolt bending.

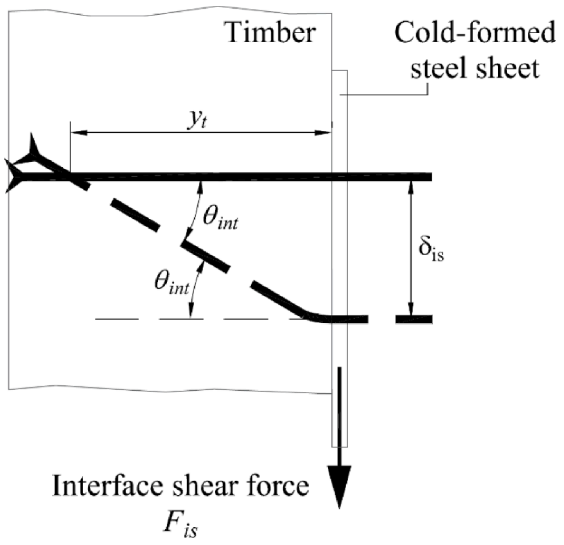

Fig. 28. Plastic hinge rotation angle θ_{int}.

pull-though tests presented in [28], by considering the increase in the head bearing area of the new fitting A_f, shown in Fig. 25, as a multiple of the screw head bearing area A_s, and accounting for a reduction in bearing strength equal to ($A^{-0.5}$), as defined for the embedment strength in Section 3:

$$f_{head,f} = f_{head,s}\left(\frac{A_f}{A_s}\right)^{-0.5} \tag{9}$$

where $f_{head,f}$ and $f_{head,s}$ are the head bearing strengths of the new bevelled head fittings and of the self-drilling screws described in [28] respectively. Besides the modifications noted above, the derivation of the axial pull-through component follows the procedure described in [29].

5.1.3. Material damage considerations

The extended model described in the previous sections consists of two force components, namely timber embedment and axial pull-through, with bending limited only to that caused on the CFS sheet, which is accounted for in the timber embedment force calculation. While the effect of damage on the axial pull-through component remains the same as that described in [29], the effect of damage on the timber embedment component is modified to account for the tolerances at the two contact boundaries, as shown in Fig. 26: (i) the tolerance between the outer surface of the fitting and the surrounding timber - a value of 0.5 mm is considered in this study; and (ii) the tolerance between the minor screw diameter d_1 and the inner fitting diameter $d_{f,i}$, where screws are utilised. The displacement in mm at which the embedment strength f_h is reached is increased by $d_{d,e}$:

$$\text{Screwed connections}: \; d_{d,e} = \frac{(d_{f,i} - d_1)}{2} + 0.5 \tag{10}$$

$$\text{Bolted connections}: \; d_{d,e} = 0.5 \tag{11}$$

5.1.4. Determination of ultimate loads and failure modes

Five possible failure modes for ordinary screw connections have been identified in previous research [29] – screw rotation, pull-through, screw bending, thread failure and screw shear failure, while a methodology for determining which mode is critical was defined. The specimens with innovative connectors investigated in this study exhibited similar modes of failure as observed in [29], plus two additional modes of

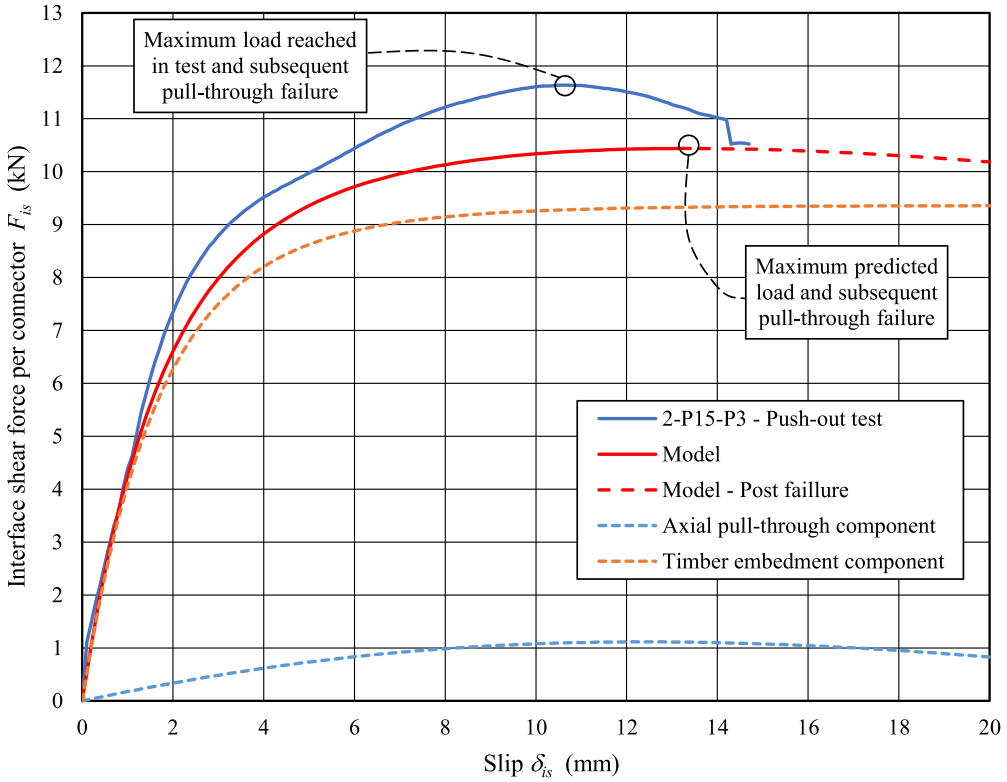

Fig. 29. Analytical prediction of the force-slip curve for specimen 2-P15-P3.

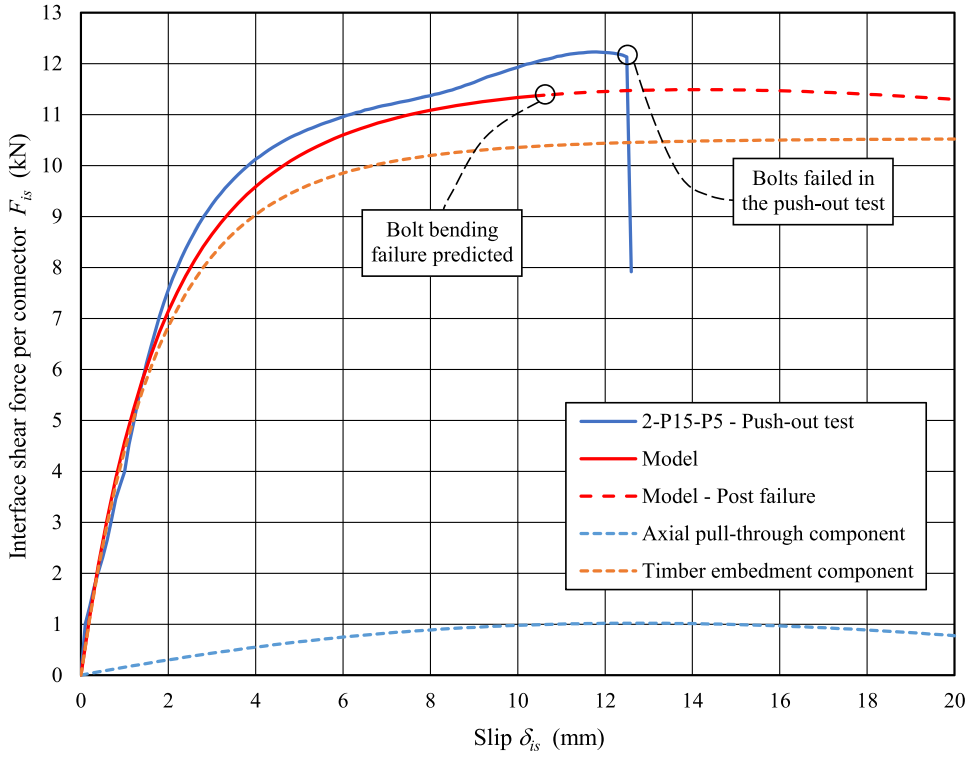

Fig. 30. Analytical prediction of the force-slip curve for specimen 2-P15-P5.

Table 6
Comparison between EN 1995–1-1 [30] predictions and test results.

Specimen designation	Test			EN 1995-1-1				
	$F_{v,t}$ (kN)	$k_{s,t}$ (N/mm)	Failure mode	$F_{v,EN}$ (kN)	$F_{v,EN}$ / $F_{v,t}$	$k_{s,EN}$ (N/mm)	$k_{s,EN}$ / $k_{s,t}$	Failure mode
2-P15-P1	6.49	1496	3, 6	6.84	1.05	28,555	19.09	1
2-P24-P1	7.63	1632	3, 6	6.84	0.90	28,555	17.50	1
2-P15-P3	11.63	3681	1, 2	6.84	0.59	28,555	7.76	1
2-P24-P3	11.21	4907	7, 1	6.84	0.61	28,555	5.82	1
2-P15-P5	12.23	3510	1/2, 3	6.84	0.56	28,555	8.14	1
2-P24-P5	11.77	4206	1/2, 3	6.84	0.58	28,555	6.79	1
2-P15-S1	7.74	2346	1, 4	6.99	0.90	28,555	12.17	1
2-P24-S1	8.74	2876	1, 4	6.99	0.80	28,555	9.93	1
2-P15-A4	11.80	4110	1, 7	6.99	0.59	28,555	6.95	1
2-P24-A4	11.78	3117	1, 7	6.99	0.59	28,555	9.16	1
2-P15-S5	12.43	3016	1, 3	6.99	0.56	28,555	9.47	1
2-P24-S5	12.33	3215	1, 3	6.99	0.57	28,555	8.88	1
				Mean	0.69	Mean	10.14	
				CoV	0.25	CoV	0.41	

Failure mode key: 1 = Fitting rotation; 2 = Pull-through failure; 3 = Screw / bolt bending failure; 4 = Screw / bolt shear failure; 5 = Thread failure; 6 = Fitting failure; 7 = Failure of locking device.

failure relating to the fitting and locking device; the applicability of the methodology presented in [29] is therefore examined herein.

A modification introduced in this study is related to the screw bending failure, particularly for those instances described in Section 5.1, where the screw or bolt is inserted into a steel fitting or steel shank and therefore bending within the connector is restrained. For these cases, if the steel sheet has a lower bending capacity $M_{pl,cfs}$ than the screw or bolt $M_{pl,conn}$, the sheet will yield, allowing the screw/bolt tip to rotate without forming a plastic hinge in the screw/bolt, as shown in Fig. 27(a). On the other hand, if the bending capacity of the steel sheet exceeds that of the screw/bolt, then a plastic hinge will form within the screw/bolt at the interface, as shown in Fig. 27(b) and the plastic hinge rotation angle θ_{int} can be calculated from the interface slip δ_{is} and the distance between the connector centroid and the shear interface y_t, as shown in Fig. 28, using Eq. (12). Screw bending failure in this case occurs when the plastic hinge rotation reaches the fracture angle obtained from three-point bending tests.

$$\theta_{int} = \tan^{-1}\left(\frac{\delta_{is}}{y_t}\right) \tag{12}$$

Comparisons of the load-slip curves generated using the extended analytical model and those from experimental results, for 2-P15-P3 and 2-P15-P5, are shown in Figs. 29 and 30 respectively. The decomposed axial pull-through and timber embedment force components are also presented.

Table 7
Comparison between analytical model predictions and test results.

Specimen designation	Test					Model								
	$F_{v,t}$ (kN)	$\delta_{is,u,,t}$ (mm)	$k_{s,t}$ (N/mm)	$k_{s,m,t}$ (N/mm)	Failure mode	$F_{v,a}$ (kN)	$F_{v,a}$ / $F_{v,t}$	$\delta_{is,u,a}$ (mm)	$\delta_{is,u,a}$ / $\delta_{is,u,t}$	$k_{s,a}$ (N/mm)	$k_{s,a}$ / $k_{s,t}$	$k_{s,m,a}$ (N/mm)	$k_{s,m,a}$ / $k_{s,m,t}$	Failure mode
2-P15-P1	6.49	6.5	1496	914	3, 6	7.25	1.12	6.8	1.05	1864	1.25	1197	1.31	3
2-P24-P1	7.63	6.9	1632	1143	3, 6	8.29	1.09	7.6	1.10	2196	1.35	1717	1.50	3
2-P15-P3	11.63	10.5	3681	3481	1, 2	10.44	0.90	13.4	1.28	4204	1.14	2786	0.80	1, 2
2-P24-P3	11.21	5.7	4907	3878	7, 1	11.30	1.01	10.6	1.86	4764	0.97	3368	0.87	1, 3
2-P15-P5	12.23	11.8	3510	3787	1/2, 3	11.38	0.93	10.6	0.90	4789	1.36	3387	0.89	1, 3
2-P24-P5	11.77	11.5	4206	3320	1/2, 3	11.99	1.02	10.6	0.92	4982	1.18	3536	1.07	1, 3
2-P15-S1	7.74	6.5	2346	1739	1, 4	9.66	1.25	7.6	1.17	3452	1.47	2147	1.23	1, 4
2-P24-S1	8.74	7.4	2876	2107	1, 4	9.65	1.10	6.4	0.86	3763	1.31	2361	1.12	1, 4
2-P15-A4	11.80	16.9	4110	1341	1, 7	10.31	0.87	13.4	0.79	3923	0.95	2561	1.91	1, 2
2-P24-A4	11.78	17.4	3117	1395	1, 7	11.08	0.94	14.2	0.82	4145	1.33	2854	2.05	1, 2
2-P15-S5	12.43	8.3	3016	4192	1, 3	11.17	0.90	10.6	1.28	4751	1.58	3352	0.80	1, 3
2-P24-S5	12.33	5.9	3215	4527	1, 3	11.82	0.96	10.6	1.80	4952	1.54	3507	0.77	1, 3
						Mean	1.01	Mean	1.15	Mean	1.29	Mean	1.19	
						CoV	0.11	CoV	0.31	CoV	0.15	CoV	0.36	

Failure mode key: 1 = Fitting rotation; 2 = Pull-through failure; 3 = Screw / bolt bending failure; 4 = Screw / bolt shear failure; 5 = Thread failure; 6 = Fitting failure; 7 = Failure of locking device.

5.2. Comparison with experimental data

In this section, the obtained test results are compared against the capacity and failure mode predictions of EN 1995–1-1 [30] and of the analytical model presented herein. Note that the values presented in Tables 6 and 7 have been derived using the average particle board embedment stress data, as presented in Fig. 8, without applying safety factors, to allow a direct comparison with the experimental results.

5.2.1. Comparison between EN 1995-1-1 [30] and experimental data

EN 1995-1-1 [30] identifies two possible failure modes for thin steel-to-timber connections in single shear, namely connector rotation and connector bending. For the connectors examined herein, when considering the bending capacity of the fitting in the connector bending expression, the results were always found to exceed those achieved using the connector rotation expression and therefore, for all cases, the governing mode of failure was connector rotation. With reference to Table 6, it can be seen that all specimens, except 2-P15-P1 and 2-P24-P1, exhibited fitting rotation as one of the failure modes and therefore the code failure mode prediction is generally accurate.

It can be seen from Table 6 that the ultimate loads $F_{v,EN}$ predicted by EN 1995–1-1 [30] are significantly lower than those measured from the push-out tests $F_{v,t}$, with a mean $F_{v,EN}/F_{v,t}$ ratio of 0.69 and a coefficient of variation (CoV) of 0.25. The predicted values of the slip modulus $k_{s,EN}$ are significantly higher than those determined from the experimental data in line with EN 26891 [33], with a mean $k_{s,EN}/k_{s,t}$ ratio of 10.14 and a CoV of 0.41.

The discrepancies in ultimate load predictions are a result of the mode of failure, and associated equations, being suggested by EN 1995-1-1 [30]. The steel sheet thickness adopted in this investigation is classified as a thin plate according to the code [30], and the equations associated with this classification assume that the connector will rotate freely at the steel-to-timber interface. The behaviour observed during push-out testing indicates however, that the steel sheet does offer some rotational restraint. The degree of this restraint defines the connector pivoting point and the extent of timber embedment. The highly unconservative slip modulus predictions, on the other hand, may not be attributed to the selected classification in EN 1995-1-1 [30], since one common expression, dependent only on the density of timber and the diameter of the connector, is given for dowels, bolts, screws and nails. The inaccuracies in this case are attributed to the failure of the code expression to take into account the steel sheet stiffness which defines the degree by which the connector rotates at the interface and therefore defines the extent of slip.

5.2.2. Comparison between proposed analytical model and experimental data

Table 7 presents a comparison between the ultimate loads, slip moduli, failure modes and slip at ultimate load, as predicted by the extended analytical model presented in Section 5.1 and as determined from the Group 2 push-out tests presented in Section 4.3. It can be seen that the proposed model can accurately predict the ultimate loads obtained experimentally, with a mean $F_{v,a}/F_{v,t}$ ratio of 1.01, a CoV of 0.11 and a maximum prediction error of 25%. Good predictions can also be noted for the slip at ultimate load $\delta_{is,u}$ and the two slip moduli k_s and $k_{s,m}$, with mean $\delta_{is,u,a}/\delta_{is,u,t}$, $k_{s,a}/k_{s,t}$, and $k_{s,m,a}/k_{s,m,t}$ ratios of 1.15, 1.29 and 1.19 respectively and with CoVs of 0.31, 0.15 and 0.36 respectively.

The failure modes predicted by the model were generally in good agreement with the observations made when assessing the test specimens. As noted in Section 5.1.4, fitting failure and failure of the locking device could not be captured by the current model and therefore constitute the only inconsistencies between the test observations and the model predictions.

6. Conclusions

An experimental investigation of bespoke CFS-to-timber shear connectors has been presented. Six connector types were first explored in a preliminary set of tests, featuring self-drilling screws or bolts, surrounded by fittings of different shapes and materials. Four of these connectors were found to be worthy of further investigation, and, thus, their behaviour was explored through a second set of tests, where the CFS thickness, fitting material and connector type were varied.

For the best performing connector, increases in ultimate load and in the slip moduli k_s and $k_{s,m}$ of around 110%, 300% and 600% respectively, were achieved compared to ordinary screw connections. This connector was also found to fulfil the requirements of ease of assembly on site, being installed perpendicular to the shear interface, requiring no access to the underside of the timber board.

An analytical model developed in previous research [29] was extended to enable the prediction of the load-slip response, ultimate load, slip moduli, failure mode and slip at ultimate load for the bespoke shear connectors presented herein. A comparison of the analytical model predictions against the experimental results revealed that the model can correctly identify the exhibited failure modes and can accurately predict the ultimate load, slip at ultimate load and the two slip moduli k_s and $k_{s,}$

$_m$, with mean model prediction-to-test ratios of 1.01, 1.15, 1.29 and 1.19 respectively.

Declaration of Competing Interest

The authors declare that they have no known competing financial interests or personal relationships that could have appeared to influence the work reported in this paper.

Data availability

Data will be made available on request.

Acknowledgements

The research work disclosed in this publication was partially funded by the ENDEAVOUR Scholarships Scheme - Group B - National Funds. The authors would like to thank Ayrshire Metals Limited for supplying the testing material and EMPAV Ltd. for machining the connectors required for the experimental program.

References

[1] Kelly A, Zweben C. Comprehensive composite materials. Pergamon Press: Elsevier; 2000.
[2] Hassanieh A, Valipour HR, Bradford MA. Load-slip behaviour of steel-cross laminated timber (CLT) composite connections. J Constr Steel Res 2016;122:110–21.
[3] Hassanieh A, Valipour HR, Bradford MA. Experimental and analytical behaviour of steel-timber composite connections. Constr Build Mater 2016;118:63–75.
[4] Ataei A, Bradford MA, Valipour HR. Sustainable high strength steel flush and plate beam-to-column composite joints with deconstructable bolted shear connectors. In: Conference: Second international conference on performance-based and lifecycle structural engineering, Brisbane, Australia; December 2015. pp. 749–757.
[5] Ataei A, Bradford MA. FE modelling of sustainable semi-rigid flush end plate composite joints with deconstructable bolted shear connectors. In: Seventh international conference on composite construction (CCVII), ASCE, Queensland, Australia; July 2013. 20 pp..
[6] Kyvelou P, Gardner L, Nethercot DA. Composite action between cold-formed steel beams and wood-based floorboards. Int J Struct Stability Dynam 2015;15(8):1540029 (17 pp.).
[7] Kyvelou P, Gardner L, Nethercot DA. Testing and analysis of composite cold-formed steel and wood-based flooring systems. J Struct Eng 2017;143(11):04017146.
[8] Kyvelou P, Gardner L, Nethercot DA. Design of composite cold-formed steel flooring systems. Structures 2017;12:242–52.
[9] Kyvelou P, Gardner L, Nethercot DA. Finite element modelling of composite cold-formed steel flooring systems. Eng Struct 2018;158:28–42.
[10] Wang X, He Q, An Z, Liu G, Wen X, Wang Y, et al. Experimental study of perfobond rib shear connector under lateral force. Appl Sci 2021;11(9088):19.
[11] Veldanda MR, Hosain MU. Behaviour of perfobond rib shear connectors: push-out tests. Can J Civ Eng 1992;19:(10 pp.).
[12] Bejtka I, Blass HJ. Joints with inclined screws. In: Proceedings, CIB-W18 timber structures, meeting 35, Paper 35-7-4; 2002.
[13] Kevarinmäki A. Joints with inclined screws. In: Proceedings, CIB-W18 timber structures, meeting 35, Paper 35-7-3; 2002.
[14] Tomasi R, Crosatti A, Piazza M. Theoretical and experimental analysis of timber-to-timber joints connected with inclined screws. Constr Build Mater 2010;24:1560–71.
[15] Jockwer R, Steiger R, Frangi A. Design model for inclined screws under varying load to grain angles. In: Proceedings, international network on timber engineering research, meeting 47, Paper 47-7-5; 2014.
[16] Girhammar UA, Jacquier N, Källsner B. Stiffness model for inclined screws in shear-tension mode in timber-to-timber joints. Eng Struct 2017;136:580–95.
[17] Jacquier N, Girhammar UA. Tests on glulam-CLT shear connections with double-sided punched metal plate fasteners and inclined screws. Constr Build Mater 2014;72:444–57.
[18] Jacquier N. Development and evaluation of mechanical joints for composite floor elements with cross laminated timber. Luleå, Sweden: Luleå University of Technology; 2015. PhD Thesis.
[19] Jacquier N, Girhammar UA. Evaluation of bending tests on composite glulam-CLT beams connected with double-sided punched metal plates and inclined screws. Constr Build Mater 2015;95:762–73.
[20] Meierhofer U. A timber/concrete composite system. Struct Eng Int 1993;3(2):104–7.
[21] Steinberg E, Selle R, Faust T. Connectors for timber-lightweight concrete composite structures. J Struct Eng 2003;129(11):1538–45.
[22] Kavaliauskas S, Kvedaras AK, Valiūnas B. Mechanical behaviour of timber-to-concrete connections with inclined screws. J Civ Eng Manag 2007;13(3):193–9.
[23] Kavaliauskas S, Kvedaras AK. The predictive model for load-carrying capacity of inclined screws as connecting-links in timber-concrete composite beams. In: 10th International conference – modern building materials, structures and techniques, Vilnius, Lithuania; May 2010. pp. 683–690.
[24] Symons D, Persaud R, Stanislaus H. Slip modulus of inclined screws in timber-concrete floors. Proc Inst Civ Eng – Struct Build 2010;163(4).
[25] Khorsandnia N, Valipour HR, Crews K. Experimental and analytical investigation of short-term behaviour of LVL-concrete composite connections and beams. Constr Build Mater 2012;37:229–38.
[26] Moshiri F, Gerber C, Valipour HR, Shrestha R, Crews KI. The predictive model for strength of inclined screws as shear connection in timber-concrete composite floor. In: Proceedings, conference on the mechanics of structures and materials; 2013. pp. 1059–1064.
[27] Krenn H, Schickhofer G. Joints with inclined screws and steel plates as outer members. In: Proceedings, CIB-W18 timber structures, meeting 42, Paper 42-7-2; 2009.
[28] Vella N, Gardner L, Buhagiar S. Experimental analysis of cold-formed steel-to-timber connections with inclined screws. Structures 2020;24:890–904.
[29] Vella N, Gardner L, Buhagiar S. Analytical modelling of cold-formed steel-to-timber connections with inclined screws. Eng Struct 2021;249.
[30] EN 1995-1-1. Eurocode 5: design of timber structures. Part 1-1: General – common rules and rules for buildings. European Committee for Standardisation, Brussels; 2004.
[31] EN 383. Timber structures – test methods – determination of embedment strength and foundation values for dowel type fasteners. Brussels, European Committee for Standardization; 2007.
[32] Ayrshire Metals Limited. Product Brochure. Available from: https://www.ayrshire.co.uk/_files/ugd/e0b978_7b9f1a5575784a699110abcc12ce68a2.pdf [Accessed July 2022].
[33] EN 26891. Timber structures – joints made with mechanical fasteners – general principles for the determination of strength and deformation characteristics. Brussels, European Committee for Standardization; 1991.
[34] Teh LH, Uz ME. Ultimate tilt-bearing capacity of bolted connections in cold-reduced steel sheets. J Struct Eng 2017;143(4). 04016206-1-04016206-12.
[35] EN 1993-1-3. Eurocode 3. Design of steel structures. General rules – supplementary rules for cold-formed members and sheeting. Brussels, European Committee for Standardization; 2005.
[36] Foschi RO. Load-slip characteristics of nails. Wood Sci 1974;7(1):69–76.